Origin of the hydrodynamic Lyapunov modes

Sean McNamara and Michel Mareschal
Centre Européen de Calcul Atomique et Moléculaire, Ecole Normale Supérieure de Lyon, 46 allée d'Italie, 69364 Lyon Cedex 07, France

(Received 5 April 2001; published 16 October 2001)

Recent studies of the Lyapunov spectrum of the hard sphere fluid reveal that there are ''hydrodynamic'' Lyapunov exponents corresponding to collective perturbations in phase space. We show that these collective perturbations are due to the conservation of certain quantities during collisions. These new conservation laws generate new hydrodynamic fields, just as the conservation of mass, momentum, and energy generate the density, velocity, and temperature fields. We then construct a detailed theory of the new hydrodynamic fields using a kinetic theory approach. This theory predicts several properties of the modes, but not all of them. This suggests that the underlying idea is correct, but a detailed theory must be elaborated in another way. The hydrodynamic exponents are not related in a simple way to the transport coefficients.

DOI: 10.1103/PhysRevE.64.051103 PACS number(s): 05.20.Dd, 05.45.Jn, 51.10.+y

I. INTRODUCTION

It is now possible to study deterministic chaos in systems with many $[O(10^3)]$ degrees of freedom. Much work has been done on the Lyapunov spectrum of these systems. These studies have resulted in a clearer understanding of the origin of irreversible, macroscopic behavior in systems with reversible microscopic dynamics. They have also established connections between the transport coefficients and the Lyapunov spectrum [1–6].

One example of this kind of study is the calculation of the Lyapunov spectrum of the hard sphere fluid [1–3]. One of the principal discoveries is the existence of ''hydrodynamic'' exponents, which correspond to collective, ''hydrodynamic'' perturbations in phase space [2]. These modes, which we will call ''hydrodynamic Lyapunov modes,'' are intriguing because they may be related to hydrodynamic fluctuations in a simple way. If it were possible to extract transport coefficients directly from these exponents, it would illuminate the relation between the reversible, microscopic dynamics and the irreversible macroscopic behavior of fluids. Two methods of relating transport coefficients to Lyapunov spectra already exist [6–8], but they involve setting up nonequilibrium simulations or locating special phase space trajectories. They do not consider the perturbations underlying the exponents. Even if the hydrodynamic Lyapunov modes have no connection to the hydrodynamic fluctuations, they are still interesting because they are responsible for the discontinuous structure of the Lyapunov spectrum near zero.

This paper is organized as follows: In Sec. II, we present a survey of the simulational results, emphasizing the hydrodynamic exponents. Some of these results have been presented elsewhere [1,2], but they are included here for completeness. The principal result is the existence of Lyapunov exponents associated with a hydrodynamic, collective perturbations. These exponents are proportional to L^{-1}, where L is the wavelength of the perturbation. In Sec. III we present a theory of the hydrodynamic exponents. Our starting point is the observation that certain quantities are conserved during collisions, and these conserved quantities give rise to new hydrodynamic fields. The hydrodynamic Lyapunov modes are the long wavelength fluctuations of these fields. We attempt to extract detailed predictions from this theory using a kinetic theory approach. The theory has a number of successes, indicating that the underlying approach is correct, but also a number of failures, suggesting that alternatives to the kinetic theory approach must be considered.

A. The hard sphere fluid

The hard sphere fluid was one of the first model fluids to be studied [9]. The collisions between the particles are assumed to be instantaneous, and to conserve energy and momentum. If the forces between two colliding particles are assumed to act only along the line connecting the particles' centers, the postcollisional velocities $\boldsymbol{v}'_{A,B}$ are given in terms of the precollisional velocities $\boldsymbol{v}_{A,B}$ by

$$\boldsymbol{v}_A{}' = \boldsymbol{v}_A + \boldsymbol{f}, \quad \boldsymbol{v}_B{}' = \boldsymbol{v}_B - \boldsymbol{f}, \quad \boldsymbol{f} \equiv (\boldsymbol{v}_B - \boldsymbol{v}_A)\cdot \hat{\boldsymbol{n}}\hat{\boldsymbol{n}}, \tag{1}$$

where the subscripts A and B label the colliding particles. The unit vector $\hat{\boldsymbol{n}}$ points from the center of particle A towards the center of particle B. In this paper, we consider the two-dimensional hard sphere fluid composed of N particles of diameter σ in a doubly periodic domain of size $L_x \times L_y$.

B. Lyapunov spectrum

The Lyapunov exponents describe how quickly two identical systems with almost identical initial conditions diverge in phase space. Consider a system at the point $\boldsymbol{\Gamma}(0)$ in phase space of L dimensions. The system follows some trajectory through phase space, arriving at $\boldsymbol{\Gamma}(t)$ at time t. We express this mathematically by defining $\mathcal{S}_t$ to be an operator that evolves a point in phase space forward a time t:

$$\boldsymbol{\Gamma}(t) = \mathcal{S}_t \boldsymbol{\Gamma}(0). \tag{2}$$

Next, consider a second system at $\boldsymbol{\Gamma} + \delta\boldsymbol{\Gamma}$, where $\delta\boldsymbol{\Gamma}$ is infinitesimally small. After a time t, this system moves to

$$\boldsymbol{\Gamma}(t) + \delta\boldsymbol{\Gamma}(t) = \mathcal{S}_t[\boldsymbol{\Gamma}(0) + \delta\boldsymbol{\Gamma}(0)]. \tag{3}$$

Then the Lyapunov exponent λ is defined to be

$$\lambda = \lim_{t\to\infty} \frac{1}{t} \ln \frac{|\delta\Gamma(t)|}{|\delta\Gamma(0)|}. \tag{4}$$

Note that λ has units of inverse time. It is thus the growth (or decay) rate of the perturbation $\delta\Gamma$. In general λ is a function of both Γ and $\delta\Gamma$. This is unfortunate, because both Γ and $\delta\Gamma$ contain L numbers, so that λ is a function on a $2L$-dimensional space. However, the situation can be improved because the $\delta\Gamma$ are infinitesimal. This means that their evolution depends only on the linearized dynamics:

$$\Gamma(t) + \delta\Gamma(t) = \mathcal{S}_t\Gamma(0) + \mathcal{M}\cdot\delta\Gamma, \tag{5}$$

where $\mathcal{M}$ is simply an $L\times L$ matrix. Since $\mathcal{M}$ is a linear operator, knowing $\lambda(\Gamma,\delta\Gamma)$ for a set of $\delta\Gamma$ that spans the phase space enables one to calculate $\lambda(\Gamma,\delta\Gamma)$ for any $\delta\Gamma$. By convention, we associate λ_1 with the fastest growing direction $\delta\Gamma_1$; λ_2 with the fastest growing direction $\delta\Gamma_2$ which is also perpendicular to $\delta\Gamma_1$ ($\delta\Gamma_1\cdot\delta\Gamma_2=0$), and λ_i with the fastest growing direction $\delta\Gamma_i$ with $\delta\Gamma_j\cdot\delta\Gamma_i=0$ for $j<i$. The vectors $\{\delta\Gamma_i\}$ are often called the ''Lyapunov vectors.''

Furthermore, for ergodic systems, the Lyapunov spectrum $\{\lambda_i\}$ is independent of Γ. This enables us to do away with the dependence on Γ, and speak about the Lyapunov spectrum of a system. A dynamical system is ergodic if its invariant distribution cannot be subdivided into smaller invariant pieces. This is a more general condition than equilibrium: systems out of equilibrium can also be ergodic, but all equilibrium systems, including the one studied in this paper, are ergodic.

C. Algorithm

The algorithm for calculating the exponents is the same as used by Dellago, Posch, and Hoover [1], which is a generalization of Benettin's algorithm for continuous-time systems [10,11]. A set of $2N$ (or $4N$) vectors $\{\delta\Gamma_i\}$ is evolved forward in time with Gram-Schmidt orthonormalization being periodically applied to $\{\delta\Gamma_i\}$. This is necessary because the vectors grow rapidly, and are attracted towards $\delta\Gamma_1$. The Lyapunov exponents are computed from the growth rates of the vectors.

All the results presented in this paper are numerical, and thus presented in dimensionless units. The particle radius defines the unit of distance and the particle mass defines the unit of mass. The unit of time is fixed by setting the average squared velocity of the particles to 1. The diameter of the disks is therefore $\sigma=2$, and the temperature of the gas is $T=1/2$ (with Boltzmann's constant $k_B=1$). We express density using the ''area fraction'' $\nu=N\pi\sigma^2/(4L_xL_y)$, the fraction of the space covered by the disks. The maximum possible value of ν is $\pi/(2\sqrt{3})\approx 0.9069$, corresponding to a hexagonal array of disks in contact.

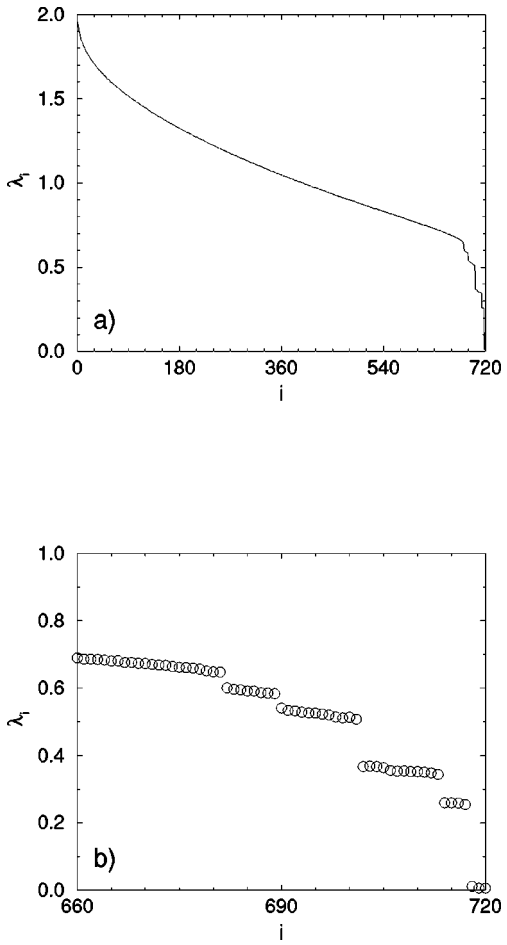

FIG. 1. The spectrum of a $N=360$ hard disk fluid in a square domain ($L_x=L_y=45=22.5\sigma$). (a) The first $2N$ Lyapunov exponents (the second $2N$ are just the negative of the exponents shown). (b) The smallest positive exponents (note difference in the x axis).

II. A SURVEY OF THE LYAPUNOV SPECTRA OF THE HARD DISK FLUID

A. System-size dependence

The Lyapunov spectrum has a special symmetry: each exponent has a partner that is exactly its negative. This is the ''conjugate pairing rule.'' [1] Therefore, it is necessary to calculate only half the spectrum. The second half contains no additional information, and is simply the negative of the first.

In Fig. 1, we show half of a typical spectrum of the hard sphere fluid at equilibrium. The parameters of the system are $N=360$, $L_x=L_y=45$. The spectrum can be divided into two parts. For $i\leqslant 681$, the exponents fall onto a well defined continuous curve. On the other hand, for $682\leqslant i\leqslant 720$, the exponents appear in small groups at discrete values. The discrete part of the spectrum corresponds to hydrodynamiclike collective perturbations, as we will show later in this section.

If the number of particles increases with density kept constant, the continuous part of the spectrum remains approximately the same, except that the exponents become more dense. The largest exponent λ_1 increases very slowly. The value of the smallest exponent in the continuous part remains constant. The discrete part of the spectrum also changes, but

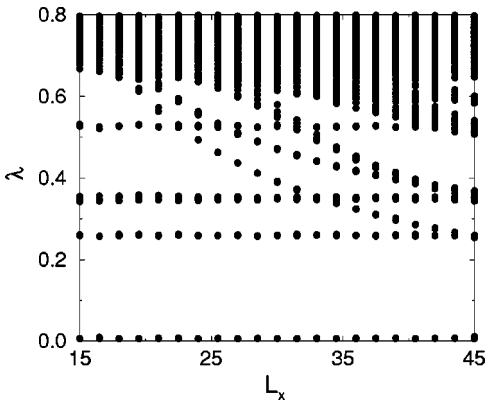

FIG. 2. The transition of the spectrum from a square ($L_x=L_y=45$) to rectangular ($L_x=15$, $L_y=45$) system. The number of particles is adjusted to keep the density equal in all simulations. The spectrum in Fig. 1 appears as a single column at $L_x=45$; for each exponent, a dot is placed on the graph. Since all those exponents have $L_x=45$, they form a single column. The spectra for the other values of L_x are displayed in the same way.

these changes depend also on the aspect ratio of the simulational domain. If we consider only square domains ($L_x=L_y$), increasing the number of particles causes each group of exponents to approach zero while remaining distinct from all the other groups. The number of exponents in each group does not change, but new groups of exponents separate from the continuous part of the spectrum. On the other hand, if the number of particles is decreased, the groups of exponents move away from zero and merge one by one with the continuous part of the spectrum. Small systems exhibit only the continuous part of the spectrum.

If one reduces L_x while keeping L_y constant, another behavior appears. Some groups of exponents increase as L_x decreases, and finally merge with the continuum. Other groups split in two parts, one of which remains independent of L_x while the other part rejoins the continuum. This process is shown in Fig. 2. We see that a long narrow system has a much simpler structure than the square system. We will therefore concentrate on the spectrum at the extreme left of Fig. 2, where only the discrete exponents independent of L_x remain. This spectrum is shown in Fig. 3.

B. General properties of the Lyapunov vectors

Now we are ready to inspect the $\delta\mathbf{\Gamma}_i$. Recall that a given particle is associated with four components of each $\delta\mathbf{\Gamma}_i$. Two components give the displacement of that particle in configuration space, and the other two give its displacement in momentum space. We denote the displacement in configuration space of particle j as $\delta\boldsymbol{r}_j^{(i)}$ and its momentum space displacement as $\delta\boldsymbol{v}_j^{(i)}$. (In the following, we always use i to denote the Lyapunov index, and j to indicate a particle.)

Armed with this notation, we can now discuss the Lyapunov vectors $\delta\mathbf{\Gamma}_i$. First, we consider the correlation between $\delta\boldsymbol{r}_j^{(i)}$ and $\delta\boldsymbol{v}_j^{(i)}$. We calculate

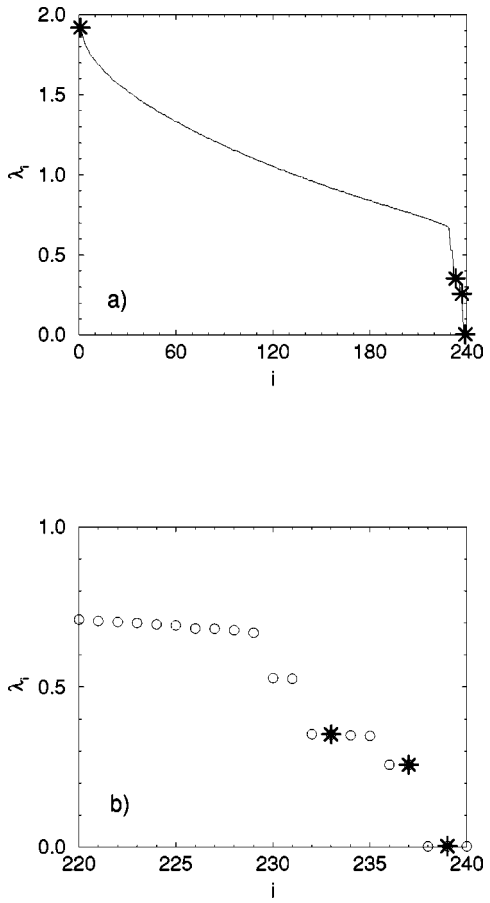

FIG. 3. The same as Fig. 1, but for an $N=120$ hard disk fluid in a rectangular domain ($L_x=15$, $L_y=45$). The density is the same as in Fig. 1, but L_x is reduced by 1/3. The stars mark the exponents featured in Fig. 5.

$$\cos\theta_{xv}=\frac{\sum_j \delta\boldsymbol{r}_j\cdot\delta\boldsymbol{v}_j}{\left[\left(\sum_j \delta\boldsymbol{r}_j^2\right)\left(\sum_j \delta\boldsymbol{v}_j^2\right)\right]^{1/2}}=\frac{\delta\mathbf{\Gamma}_x\cdot\delta\mathbf{\Gamma}_v}{|\delta\mathbf{\Gamma}_x||\delta\mathbf{\Gamma}_v|}. \quad (6)$$

We have divided the $4N$-dimensional vector $\delta\mathbf{\Gamma}_i$ into two parts $\delta\mathbf{\Gamma}_x$ and $\delta\mathbf{\Gamma}_v$. $\delta\mathbf{\Gamma}_x$ contains the configuration space displacements $\delta\boldsymbol{r}_j^{(i)}$, and $\delta\mathbf{\Gamma}_v$ the velocity-space displacements $\delta\boldsymbol{v}_j^{(i)}$. $\delta\mathbf{\Gamma}_x$ and $\delta\mathbf{\Gamma}_v$ are both $2N$ component vectors and we can consider them existing in the same $2N$-dimensional space, with the angle between them being θ_{xv}. In Fig. 4, we see that this angle is always small (i.e., $\cos\theta_{xv}\sim 1$) when $i<2N$. This is especially true when i is close to $2N$. Therefore, when investigating the $\delta\mathbf{\Gamma}$, it suffices to examine the configuration space displacement components, because the velocity displacements are similar. This similarity between the velocity and position displacements was noted by the first paper that studied Lyapunov exponents numerically [4].

A Lyapunov vector is closely related to its conjugate. Consider an exponent λ and its vector $\delta\mathbf{\Gamma}$. As stated at the beginning of this section, each exponent has a ''conjugate'' partner λ^* with a vector $\delta\mathbf{\Gamma}^*$ such that $\lambda^*=-\lambda$. This con-

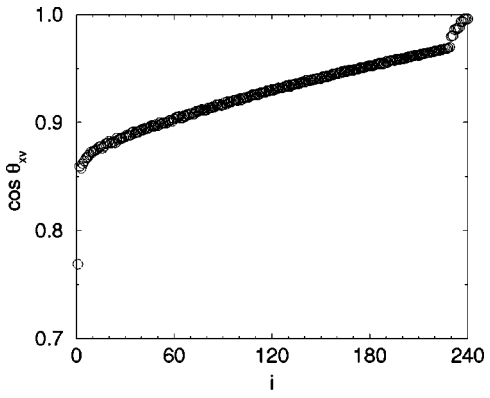

FIG. 4. The angle between $\delta\mathbf{\Gamma}_x$ and $\delta\mathbf{\Gamma}_v$ (see text) for the spectrum shown in Fig. 3 ($N=120, L_x=15, L_y=45$). For $i<2N$, $\delta\mathbf{\Gamma}_x$ and $\delta\mathbf{\Gamma}_v$ are always nearly parallel, especially for i near $2N$. When $i>2N$, $\delta\mathbf{\Gamma}_x$ and $\delta\mathbf{\Gamma}_v$ are always nearly antiparallel (not shown). Note the curious behavior of the largest exponent ($i=1$), which is detached from the other exponents. As density is decreased, we always observe that $\cos\theta_{xv}>0.8$, except the for largest, $i=1$, exponent.

jugate pairing rule holds for all Hamiltonian systems, and follows from time reversibility: if two trajectories separate exponentially in time, reversing the direction of time, (and thus the direction of the trajectories), will cause them to approach one another exponentially. We find that $\delta\mathbf{\Gamma}$ is related to $\delta\mathbf{\Gamma}^*$ by

$$\delta\mathbf{\Gamma}_x^* = \delta\mathbf{\Gamma}_v\,, \quad \delta\mathbf{\Gamma}_v^* = -\delta\mathbf{\Gamma}_x\,. \tag{7}$$

Note that the position and velocity coordinates exchange places. This relation is observed very accurately (to more than eight decimal places for some pairs). But this accuracy is very sensitive to the presence of other exponents. When two exponents are close together, Eq. (7) is much less accurate, or even false, probably because the vectors of the two exponents can be mixed together.

Note that Eq. (7) shows that the simple explanation of the conjugate pairing rule given above is not true. If reversing time simply reversed the direction of the trajectories, Eq. (7) would be $\delta\mathbf{\Gamma}_x^* = \delta\mathbf{\Gamma}_x$, and $\delta\mathbf{\Gamma}_v^* = -\delta\mathbf{\Gamma}_v$, i.e., the position displacements would be unchanged and the velocity displacements reversed. Reversing the direction of time does not change the central trajectory $\mathbf{\Gamma}(t)$; it is simply traced backwards in time. But the ''satellite'' trajectories $\mathbf{\Gamma}(t) + \delta\mathbf{\Gamma}_i(t)$ do change; they are not simply reversed.

C. Characterization of the Lyapunov vectors

Turning our attention to individual exponents, we can readily discern the physical meanings of the six zero exponents.

The ''position displacement'' exponents: these two zero exponents have $\delta\boldsymbol{r}_j = \boldsymbol{A}$, where $\boldsymbol{A}$ is a constant vector, independent of j. This perturbation consists of displacing all the particles equally in the direction of $\boldsymbol{A}$. The sequence of collisions is not changed; the location of each collision is merely translated in space. These two exponents are a consequence of the translational invariance of the laws governing the motion of the particles. There are two exponents because there are two independent directions available.

The ''velocity displacement'' exponents: these two zero exponents have $\delta\boldsymbol{v}_j = \boldsymbol{A}$, where $\boldsymbol{A}$ is again a constant vector, independent of j. This perturbation corresponds to changing the velocity of the center of mass without changing the relative velocity of any of the particles. Again, the sequence of collisions does not change. These exponents express Galilean invariance.

The ''time displacement'' exponent: this exponent has $\delta\boldsymbol{r}_j = a\boldsymbol{v}_j$, where $\boldsymbol{v}_j$ is the velocity of particle j and a is a scalar. This perturbation corresponds to perturbing the system in the direction of its trajectory in phase space. The collisions in the perturbed system will occur slightly earlier (or later, depending on the sign of a) than in the unperturbed system. This exponent expresses time translational invariance.

The ''energy displacement'' exponent: this last exponent has $\delta\boldsymbol{v}_j = a\boldsymbol{v}_j$, and corresponds to multiplying the velocity of each particle by a factor. The perturbed and unperturbed systems both have the same sequence of collisions, but one has a higher collision frequency than the other. The two systems separate in phase space, but only linearly. The Lyapunov exponent, which measures exponential separation, is still zero. This exponent is a consequence of the linearity of the collision rule, Eq. (1), in $\boldsymbol{v}$.

We now investigate the nonzero exponents by projecting the $\delta\boldsymbol{r}_j$ onto the positions of the corresponding particles. This is done in Fig. 5, where we show four typical vectors, one from the continuous part of the spectrum, and the rest from the discrete part.

The continuous part of the spectrum [represented by $\delta\mathbf{\Gamma}_1$ in Fig. 5(a)] corresponds to disorganized and local perturbations. Many particles have very small contributions to $\delta\mathbf{\Gamma}_1$. As the Lyapunov index i increases, the modes become less local: more and more particles have significant amplitudes. However, the modes remain disorganized. These modes are also very time dependent. If the simulation were to run a bit longer or a bit shorter, the set of contributing particles would change, and Fig. 5(a) would look completely different. On the other hand, if the calculation were started with a different initial $\delta\mathbf{\Gamma}_1$ (but the same initial particle velocities and positions, i.e., the same initial $\mathbf{\Gamma}$) and run for the same length of time, Fig. 5(a) would not change at all.

In the discrete part of the spectrum, the exponents correspond to collective motions of the particles. This explains why these exponents appear in small separated groups at discrete values. For example, $\lambda_{236}=\lambda_{237}$ (in the limit of an average over an infinitely long time) because both exponents correspond to transverse, sinusoidal shearing perturbations [$\delta\mathbf{\Gamma}_{237}$ is shown in Fig. 5(d), and $\delta\mathbf{\Gamma}_{236}$ is the same, but with a phase shift of $\pi/2$]. Higher harmonics of the shear waves also exist. The pair of exponents λ_{231} and λ_{230} correspond to transverse shear waves with a wavelength of $L_y/2$. Note also that $\lambda_{230}=\lambda_{231}\approx 2\lambda_{237}$. As L_y is increased further, it is possible to see the third harmonic, then the fourth, and so on.

The exponents λ_{232} through λ_{235} corresponds to longitudinal waves, where compressive motion is coupled to a heat-

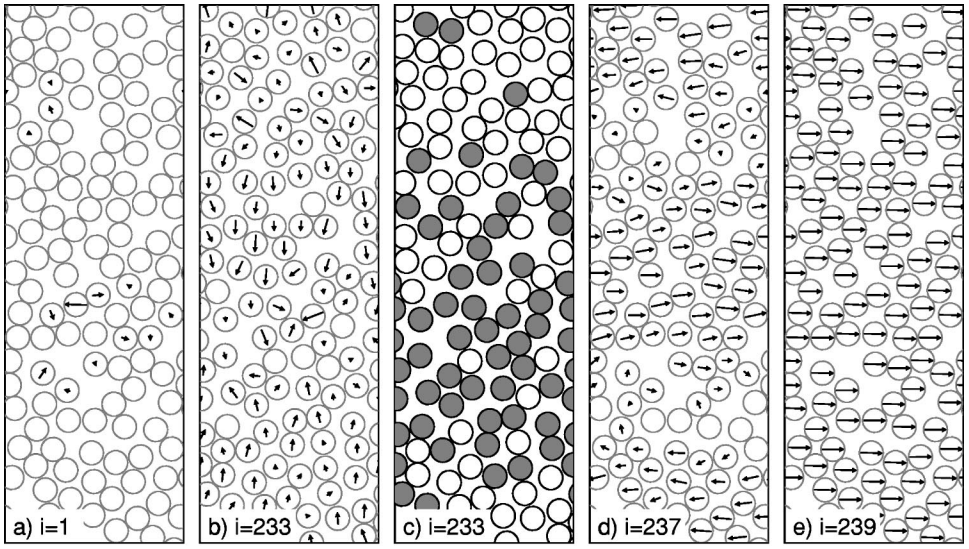

FIG. 5. Lyapunov vectors corresponding to λ_1, λ_{233}, λ_{237}, and λ_{239} of the hard disk fluid whose spectra is shown in Fig. 3 ($N=120$, $L_x=15$, and $L_y=45$). The circles show the positions of the particles at the end of the simulation. In panels (a), (b), (d), and (e), the arrows show $\delta \boldsymbol{r}_j^{(i)}$, the components of $\delta\boldsymbol{\Gamma}_i$ that describe the configuration space displacement of particle j. (The velocity space displacements are nearly equivalent.) The lengths of the vectors are scaled by the maximum length. If the length of a vector is less than 0.16, no vector is shown. In panel (c), we shade the particles with $\delta \boldsymbol{r}_j \cdot \boldsymbol{v}_j > 0$.

ing or cooling of the gas. (In Fig. 5, we show position perturbations $\delta \boldsymbol{r}_j$ not velocity perturbations $\delta \boldsymbol{v}_j$, but for nonzero vectors, these two quantities are closely correlated.) These waves resemble sound waves, but they do not have the same relation between velocity and position displacements. In true sound waves, the velocity and position displacements are out of phase, but in the longitudinal Lyapunov waves, the two displacements have the same phase. Furthermore, these waves do not propagate at the sound speed, but they do have higher harmonics just as the shear waves. Nevertheless, we will refer to these Lyapunov modes as ''sound modes.''

For long, rectangular systems, the Lyapunov exponents in the discrete part of the spectrum obey

$$\lambda = \frac{n c_\lambda}{L_y} + \frac{n^2 d_\lambda}{L_y^2} + O(1/L_y^3), \quad n = 0,1,\ldots, \tag{8}$$

where n is the mode number. (The zero modes can be considered the $n=0$ members of this series.) The upper limit on n is fixed by the continuous part of the spectrum. When the exponent predicted by Eq. (8) falls in the continuous part of the spectrum, it no longer exists as a discrete mode. The first term in Eq. (8) also appears in a mathematical model of the Lyapunov exponents [12], where the evolution of $\{\delta\boldsymbol{\Gamma}\}$ is modeled by generating and applying random matrices of a form consistent with the physics. Note that c_λ has dimensions of velocity and d_λ of a diffusivity. These two quantities depend on density and on whether one considers a sound or shearing mode.

The structure of the discrete part of the spectrum can be explained by Eq. (8), together with the observation that each possible wavenumber vector $\boldsymbol{k}$ generates six exponents: two shearing modes and four sound modes. In narrow rectangular systems (as in Figs. 3 and 5), $\vec{k}$ is parallel to the y axis: $\boldsymbol{k} = (2\pi n/L_y)\hat{\boldsymbol{y}}$. One could also take $\boldsymbol{k} = (2\pi n/L_x)\hat{\boldsymbol{x}}$, but these exponents are lost in the continuous part of the spectrum. As L_x is increased, the exponents generated by $\boldsymbol{k} = (2\pi n/L_x)\hat{\boldsymbol{x}}$ decrease, emerge from the continuum, and join those generated by $\boldsymbol{k} = (2\pi n/L_y)\hat{\boldsymbol{y}}$ when $L_x = L_y$. This process can be seen in Fig. 2. It is also possible that $\boldsymbol{k}$ be oriented diagonally. This complicates the spectrum of square systems.

But Eq. (8) renders interpretation of the hydrodynamic Lyapunov modes difficult. The simplest idea is that the collective perturbations in phase space are equivalent to collective perturbations in velocity space, i.e., the shear wave of Fig. 5(d) is equivalent to imposing a infinitesimally small sinusoidal shearing perturbation on a fluid in equilibrium. The phase space perturbation would then decay at the same rate as the hydrodynamic one, with $\lambda \sim 1/L^2$. This would establish a simple and direct link between the transport coefficients (such as the viscosity) and the Lyapunov spectrum. However, this interpretation is excluded by Eq. (8) because $\lambda \sim 1/L$.

We have measured c_λ and d_λ for a range of densities by running a series of simulations with the same density but different L_y and then measuring the exponent of the $n=1$ waves. Plotting λL_y against $1/L_y$ gives a straight line with slope d_λ and intercept c_λ. In Fig. 6(a), we show the values of c_λ measured by this method.

In Fig. 6(b), we show d_λ as a function of density. This quantity is much more difficult to measure than c_λ, because one must measure small changes in λL_y as L_y becomes large and λ becomes small. Small errors in λ cause large errors in d_λ. Also, for $0.25 \leqslant \nu \leqslant 0.35$, the shear and sound modes are quite close together, and they can mix with each other, further complicating the analysis. Nevertheless, certain trends emerge from the data. The most evident is that $d_\lambda > 0$. The

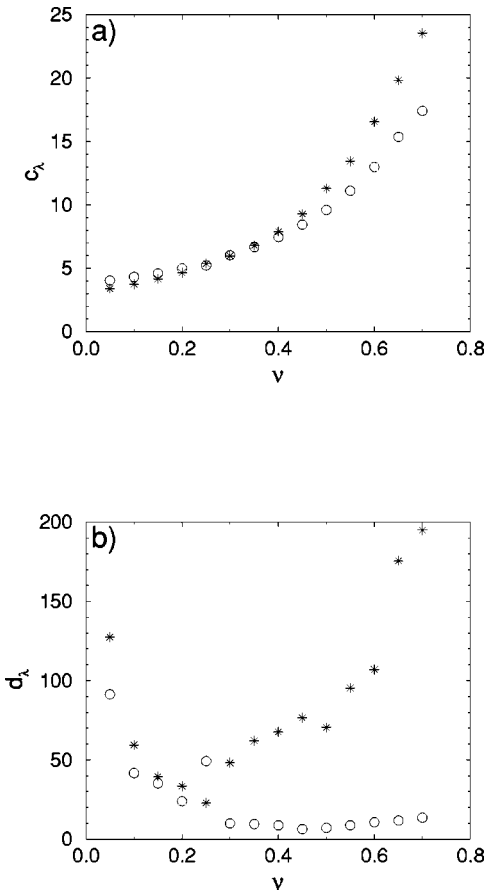

FIG. 6. The dependence of c_λ and d_λ in Eq. (8) as a function of the area fraction ν. The circles correspond to the shearing mode [an example is shown in Fig. 5(d)], and the stars correspond to the soundlike modes [an example is shown in Figs. 5(b, c)]. At each density, several simulations were done, permitting c_λ and d_λ to be estimated using Eq. (8).

diffusivity does not represent a kind of damping that counters the $O(1/L_y)$ growth of the perturbation. At small densities, d_λ seems to diverge. Note that c_λ tends to a constant as $\nu \to 0$. Thus at very small densities and finite wavelengths, the quadratic term in Eq. (8) may dominate. At large densities, the two types of modes have very different values of d_λ: the diffusivity of the sound modes may diverge while the d_λ of the shear modes approaches a constant.

III. A THEORY FOR THE HYDRODYNAMIC LYAPUNOV MODES

In this section, we develop a theory of the ''hydrodynamic'' exponents. The theory explains why the growth rates are proportional to $1/L_y$, what the mechanism of the growth is, and why two types of modes appear. Our theory parallels the derivation of the usual hydrodynamic equations from the Boltzmann equations. First, we consider $\delta \boldsymbol{r}_j$ and $\delta \boldsymbol{v}_j$ as vector quantities carried by the particle j. We identify six functions of $\delta \boldsymbol{r}$ and $\delta \boldsymbol{v}$ that are conserved during collisions. These six quantities are associated with the six zero modes discussed in Sec. II C, and give rise to six new hydrodynamic fields. Next, we derive equations for each of these new fields. When we consider linear, sinusoidal perturbations of these fields, two equations decouple from the other four. The two decoupled equations give rise to the shear waves while the other four are the origin of the sound waves.

As with the usual hydrodynamic equations, the resulting equations are not closed: they contain higher moments. We make a simple closure hypotheses: that the hydrodynamic fields contain all the information about the correlation between the perturbations $\delta \boldsymbol{r}$ and $\delta \boldsymbol{v}$, and the velocity $\boldsymbol{v}$. Using this assumption, we are able to calculate the collisional fluxes of the conserved quantities, and we find a negative diffusion constant that explains the growth of the shear modes. The theory is unable to explain the growth of the sound modes, although it accurately predicts their frequency.

A. The hydrodynamic fields

It is possible to show that during collisions, the perturbation in position, $\delta \boldsymbol{r}$, follows the same transformation rule as the velocities given in Eq. (1),

$$\delta \boldsymbol{r}_A' = \delta \boldsymbol{r}_A + \boldsymbol{f}_r, \quad \delta \boldsymbol{r}_B' = \delta \boldsymbol{r}_B - \boldsymbol{f}_r, \quad \boldsymbol{f}_r \equiv (\delta \boldsymbol{r}_B - \delta \boldsymbol{r}_A)\cdot \hat{\boldsymbol{n}}\hat{\boldsymbol{n}}, \tag{9}$$

where the primes indicate postcollisional quantities. On the other hand, when one considers the velocity perturbation, two terms appear in $\boldsymbol{f}_c$:

$$\delta \boldsymbol{v}_A' = \delta \boldsymbol{v}_A + \boldsymbol{f}_v, \quad \delta \boldsymbol{v}_B' = \delta \boldsymbol{v}_B - \boldsymbol{f}_v,$$

$$\boldsymbol{f}_v \equiv (\delta \boldsymbol{v}_B - \delta \boldsymbol{v}_A)\cdot \hat{\boldsymbol{n}}\hat{\boldsymbol{n}} + V\sigma^{-1}\sec\theta\,(\delta \boldsymbol{r}_B - \delta \boldsymbol{r}_A)\cdot \hat{\boldsymbol{u}}\hat{\boldsymbol{u}}', \tag{10}$$

where $V \equiv |\boldsymbol{v}_A - \boldsymbol{v}_B|$ and θ is the angle between $\boldsymbol{v}_B - \boldsymbol{v}_A$ and $\hat{\boldsymbol{n}}$. We define the unit vector $\hat{\boldsymbol{t}}$ such that $\hat{\boldsymbol{n}}\cdot\hat{\boldsymbol{t}} = 0$ and $\hat{\boldsymbol{n}}\times\hat{\boldsymbol{t}} = 1$. (Here, we define the cross product to be a scalar: $\boldsymbol{a}\times\boldsymbol{b} \equiv a_x b_y - a_y b_x$. If our two-dimensional space were embedded in three dimensions, $\boldsymbol{a}\times\boldsymbol{b}$ would be the z component of the usual vector cross product.) We define $\hat{\boldsymbol{u}}$ to be a unit vector perpendicular to the precollisional relative velocity and $\hat{\boldsymbol{u}}'$ to be perpendicular to the postcollisional relative velocity, so that $(\boldsymbol{v}_B - \boldsymbol{v}_A)\times\hat{\boldsymbol{u}} = (\boldsymbol{v}_B' - \boldsymbol{v}_A')\times\hat{\boldsymbol{u}}' = |\boldsymbol{v}_B - \boldsymbol{v}_A| = V$. Figure 7 summarizes these definitions.

The first term of $\boldsymbol{f}_v$ in Eq. (10) has the same form as of $\boldsymbol{f}_r$ and $\boldsymbol{f}$. But there is a second term that depends in a complicated way on the geometry of the collision: This new term is very important, because it is responsible for the exponential growth of the phase space perturbations. It becomes very large when $\theta \to \pi/2$ or $\theta \to -\pi/2$, i.e., when the collisions are nearly tangential.

Using Eqs. (1), (9), and (10) one can show that certain quantities are conserved during collisions:

$$\delta \boldsymbol{r}_A' + \delta \boldsymbol{r}_B' = \delta \boldsymbol{r}_A + \delta \boldsymbol{r}_B,$$

$$\delta \boldsymbol{v}_A' + \delta \boldsymbol{v}_B' = \delta \boldsymbol{v}_A + \delta \boldsymbol{v}_B,$$

$$\boldsymbol{v}_A'\cdot\delta \boldsymbol{r}_A' + \boldsymbol{v}_B'\cdot\delta \boldsymbol{r}_B' = \boldsymbol{v}_A\cdot\delta \boldsymbol{r}_A + \boldsymbol{v}_B\cdot\delta \boldsymbol{r}_B,$$

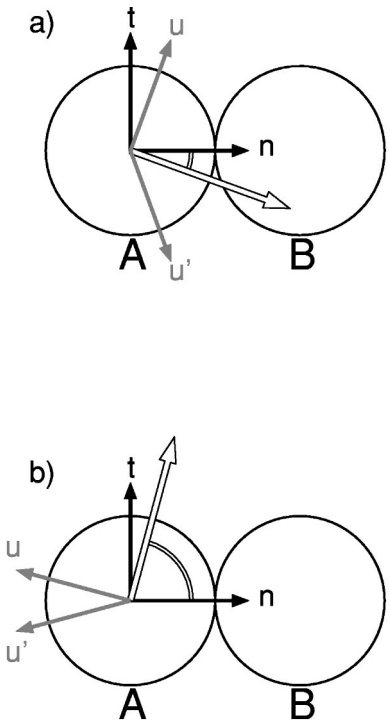

FIG. 7. The unit vectors $\hat{\boldsymbol{n}}$, $\hat{\boldsymbol{t}}$, $\hat{\boldsymbol{u}}$, and $\hat{\boldsymbol{u}}'$ for two different collisions. The wide white vector is $\boldsymbol{v}_A-\boldsymbol{v}_B$. The angle θ is indicated by the double arc between $\hat{\boldsymbol{n}}$ and $\boldsymbol{v}_A-\boldsymbol{v}_B$. In panel (a) $\theta=-20°$, and in panel (b) $\theta=75°$.

$$\boldsymbol{v}_A'\cdot\delta\boldsymbol{v}_A'+\boldsymbol{v}_B'\cdot\delta\boldsymbol{v}_B'=\boldsymbol{v}_A\cdot\delta\boldsymbol{v}_A+\boldsymbol{v}_B\cdot\delta\boldsymbol{v}_B. \tag{11}$$

These conserved quantities correspond to the six zero exponents discussed in Sec. II C. The first conserved quantity $\delta\boldsymbol{r}$ corresponds to the position displacement exponents. The second quantity, $\delta\boldsymbol{v}$ corresponds to the velocity displacement exponents. The dot products $\boldsymbol{v}\cdot\delta\boldsymbol{r}$ and $\boldsymbol{v}\cdot\delta\boldsymbol{v}$ correspond to the time and energy displacement exponents, respectively. As we will see, the six conserved quantities in Eq. (11) are microscopic quantities that underlie six new hydrodynamic fields. Recall that hydrodynamic modes exist in ordinary fluids because particle interactions conserve certain quantities. For example, momentum cannot be created or destroyed by collisions. Thus, a local concentration of momentum decays slowly because the collisions cannot destroy momentum; the momentum must be transported by diffusion. In the same way, introducing a local concentration of any of the quantities in Eq. (11) will change slowly since none of these quantities can be destroyed by collisions. We would therefore like to construct hydrodynamic equations for the coarse-grained fields corresponding to the conserved quantities. Let us define the new hydrodynamic fields $\boldsymbol{X}$, $\boldsymbol{U}$, D, and E:

$$n\boldsymbol{X}=\langle\delta\boldsymbol{r}\rangle,\quad n\boldsymbol{U}=\langle\delta\boldsymbol{v}\rangle,\quad nD=\langle\boldsymbol{v}\cdot\delta\boldsymbol{r}\rangle,\quad nE=\langle\boldsymbol{v}\cdot\delta\boldsymbol{v}\rangle. \tag{12}$$

Here, the angular brackets signify an average over the particles in a small area, and n is the number density. The usual hydrodynamic fields would be written in this notation as

$$n=\langle 1\rangle,\quad n\boldsymbol{u}=\langle\boldsymbol{v}\rangle,\quad nT=\tfrac{1}{2}\langle(\boldsymbol{v}-\boldsymbol{u})^2\rangle. \tag{13}$$

These definitions assume that all particles have the same mass. When the particles have different masses, it becomes more convenient to use the mass density ρ instead of the number density n.

There is one difference between Eq. (12) and Eq. (13). In Eq. (13), all the conserved quantities are conserved by both the collisions and the free motion of the particles. This is not so in Eq. (12) for $\boldsymbol{X}$ and D change during the free motion where $\delta\dot{r}=\delta\boldsymbol{v}$. However, since $\delta\boldsymbol{v}$ and $\delta\boldsymbol{r}$ are roughly parallel (as shown in Fig. 4), the free motion simply multiplies $\boldsymbol{X}$ and D by a constant. Furthermore, this change of $\delta\boldsymbol{r}$ during the free motion of the particles will be taken into account in the next section.

We will analyze the hydrodynamic Lyapunov modes as sinusoidal perturbations of the new hydrodynamic fields given in Eq. (12). For example, the mode shown in Fig. 5(d) is a perturbation of $\boldsymbol{X}$ with a wavelength equal to L_y. Figures 5(b) and 5(c), show that $\delta\boldsymbol{\Gamma}_{233}$ involves sinusoidal perturbations of both $\boldsymbol{X}$ [Fig. 5(b)] and D [Fig. 5(c)]. We will next use kinetic theory to construct equations governing the new hydrodynamic fields. These equations will explain the appearance of two shear modes and four soundlike modes at each wavelength.

B. The hydrodynamic equations

We will derive equations for the new hydrodynamic fields from a generalized Boltzmann equation,

$$\frac{\partial\phi}{\partial t}+\boldsymbol{v}\cdot\boldsymbol{\nabla}_{\boldsymbol{r}}\phi+\delta\boldsymbol{v}\cdot\boldsymbol{\nabla}_{\delta\boldsymbol{r}}\phi=\mathcal{C}, \tag{14}$$

where the generalized distribution function

$$\phi=\phi(\boldsymbol{v},\delta\boldsymbol{r},\delta\boldsymbol{v},\boldsymbol{r},t) \tag{15}$$

gives the density of particles with velocity $\boldsymbol{v}$ and carrying the perturbations $\delta\boldsymbol{r}$ and $\delta\boldsymbol{v}$ at position $\boldsymbol{r}$ at time t. The generalized distribution function ϕ is related to the familiar velocity distribution function f of kinetic theory by

$$f(\boldsymbol{v})=\int\int\phi\,d\delta\boldsymbol{r}\,d\delta\boldsymbol{v}=\frac{n}{2\pi T}e^{-v^2/2T}. \tag{16}$$

We have set f equal to the Maxwellian, because we are only concerned with equilibrium systems in this paper. The Lyapunov coordinates are coupled to the physical ones in ways that will be discussed below. The notation $\nabla_{\boldsymbol{r}}\phi$ in Eq. (14) indicates the gradient of ϕ with respect to $\boldsymbol{r}$ and $\nabla_{\delta\boldsymbol{r}}\phi$ indicates the gradient of ϕ with respect to $\delta\boldsymbol{r}$. The third term on the left represents the streaming motion between collisions when $\delta\dot{\boldsymbol{r}}=\delta\boldsymbol{v}$. The term on the right-hand side gives the change in ϕ induced by collisions:

$$\mathcal{C}(\boldsymbol{q},\boldsymbol{r},t)=\sigma\int \phi_A(\boldsymbol{r})\phi_B(\boldsymbol{r})[\,\delta(\boldsymbol{q}_A'-\boldsymbol{q})-\delta(\boldsymbol{q}_A-\boldsymbol{q})\,]V \times\cos\theta d\boldsymbol{q}_B d\theta. \tag{17}$$

To lighten the notation, we have used $\boldsymbol{q}$ to indicate the coordinates $\boldsymbol{v}$, $\delta\boldsymbol{r}$, and $\delta\boldsymbol{v}$, and the subscript on ϕ to show which particle it represents:

$$\boldsymbol{q}_i=(\boldsymbol{v}_i,\delta\boldsymbol{r}_i,\delta\boldsymbol{v}_i),$$

$$d\boldsymbol{q}_i=d\boldsymbol{v}_i\,d\,\delta\boldsymbol{r}_i\,d\,\delta\boldsymbol{v}_i,$$

$$\phi_i(\boldsymbol{r})=\phi(\boldsymbol{q}_i,\boldsymbol{r},t). \tag{18}$$

$\mathcal{C}$ is an integral over all possible collisions. The colliding particles and their coordinates are labeled A and B, as in Fig. 7. The delta functions select certain collisions. The first delta function selects those collisions where the postcollisional coordinates of A are equal to $\boldsymbol{q}$. The second delta function selects collisions where the precollisional coordinates of A are $\boldsymbol{q}$. These two delta functions generate the gain and loss terms of the collision operator. Finally $V\cos\theta$ gives the frequency of collision. As in Fig. 7, $V=|\boldsymbol{v}_A-\boldsymbol{v}_B|$ and θ is the angle between $\boldsymbol{v}_A-\boldsymbol{v}_B$ and $\hat{\boldsymbol{n}}$. For a collision to be possible, $-\pi/2\leqslant\theta\leqslant\pi/2$. The unit vector $\hat{\boldsymbol{n}}$ is shown in Fig. 7; it always points towards particle B.

We will not solve the Eq. (14) for ϕ but rather use it to derive equations for the new hydrodynamic fields. Let ψ be any of the quantities in the angular brackets in Eq. (12) or Eq. (13). Multiply the Boltzmann equation (14) by ψ and integrate over $\boldsymbol{q}$. The result is

$$\frac{\partial\langle\psi\rangle}{\partial t}+\boldsymbol{\nabla}\cdot\langle\boldsymbol{v}\,\psi\rangle+\langle\psi\delta\boldsymbol{v}\cdot\boldsymbol{\nabla}_{\delta\boldsymbol{r}}\phi\rangle=\langle\psi\mathcal{C}\rangle. \tag{19}$$

The first term on the left-hand side is the time rate of change of n times one of the hydrodynamic fields. The second term gives the streaming transport of ψ. The third term vanishes unless ψ depends on $\delta\boldsymbol{r}$. This term reflects the amplification of $\delta\boldsymbol{r}$ by $\delta\boldsymbol{v}$ during the free motion. The right-hand side is the collisional change of ψ. This last term can be simplified to

$$\langle\psi\mathcal{C}\rangle=\frac{\sigma}{2}\int[\,\psi_A'+\psi_B'-\psi_A-\psi_B]\phi_A(\boldsymbol{r})\phi_B(\boldsymbol{r})V \times\cos\theta d\boldsymbol{q}_A d\boldsymbol{q}_B d\theta, \tag{20}$$

where $\psi_i=\psi(\boldsymbol{q}_i)$, and the definitions of Eq. (18) have been used again. Now, the significance of Eq. (11) becomes clear. When ψ is any of the conserved quantities, $\langle\psi\mathcal{C}\rangle$ vanishes. Setting ψ equal to each of the conserved quantities, Eq. (19) generates the following equations:

$$\frac{\partial\boldsymbol{X}}{\partial t}+\boldsymbol{\nabla}\cdot\langle\boldsymbol{v}\,\delta\boldsymbol{r}\rangle=\boldsymbol{U},$$

$$\frac{\partial\boldsymbol{U}}{\partial t}+\boldsymbol{\nabla}\cdot\langle\boldsymbol{v}\,\delta\boldsymbol{v}\rangle=0,$$

$$\frac{\partial D}{\partial t}+\boldsymbol{\nabla}\cdot\langle\boldsymbol{v}(\boldsymbol{v}\cdot\delta\boldsymbol{r})\rangle=E,$$

$$\frac{\partial E}{\partial t}+\boldsymbol{\nabla}\cdot\langle\boldsymbol{v}(\boldsymbol{v}\cdot\delta\boldsymbol{v})\rangle=0. \tag{21}$$

The quantities in angular brackets are the streaming fluxes. They give the transport of the concerned quantity by the free motion of the particles. To get a set of closed equations, we must make a closure hypothesis, relating the streaming fluxes to the hydrodynamic fields.

We will use the simplest possible closure hypothesis that is consistent with the existence of the hydrodynamic fields. We assume that all the correlations between Lyapunov degrees of freedom and the physical ones vanish, except the correlations described by D and E. We also exploit the fact that the physical variables are set by thermal equilibrium, so that n and T are independent of position and $\langle\boldsymbol{v}\rangle=0$. To start with, we have

$$\langle v_y\delta r_x\rangle=\langle v_x\delta r_y\rangle=\langle v_x\rangle\langle\delta r_y\rangle=0. \tag{22}$$

The average can be separated because there is no hydrodynamic variable that describes this correlation. Finally, the product vanishes because $\langle\boldsymbol{v}\rangle=0$. The accuracy of this assumption can be estimated by quantities such as

$$\delta=\frac{\langle v_y\delta r_x\rangle}{\langle v\rangle\langle\delta r_x\rangle}, \tag{23}$$

where $\langle v\rangle=\langle\sqrt{v_x^2+v_y^2}\rangle=1$. When considering a streaming flux, such as $\langle v_y\delta r_x\rangle$, we have $\delta<0.10$, [$\delta\approx0.07$ for Fig. 5(d)] but δ decreases as the wavelength of the perturbation increases. For quantities such as $\langle v_x\delta r_y\rangle$ that are not streaming fluxes, δ is very small; $\delta<0.05$ and often $\delta<0.01$.

On the other hand, correlations such as $\langle v_x\delta r_x\rangle$ do not vanish because they are related to the hydrodynamic field D,

$$\langle v_x\delta r_x\rangle=\langle v_y\delta v_y\rangle=\frac{nD}{2}. \tag{24}$$

We assume that $\langle v_x\delta r_x\rangle=\langle v_y\delta v_y\rangle$, because otherwise another quantity $\langle v_x\delta r_x-v_y\delta v_y\rangle$ would be needed to describe the correlations between $\delta\boldsymbol{r}$ and $\boldsymbol{v}$. Analogous arguments lead to $\langle v_x\delta v_x\rangle=\langle v_y\delta v_y\rangle=nE/2$. Equation (24) is the most doubtful assumption of the closure hypothesis, for the sound modes typically have

$$\frac{\langle v_x\delta r_x-v_y\delta v_y\rangle}{\langle v_x\delta r_x+v_y\delta v_y\rangle}\sim0.2. \tag{25}$$

Considering higher powers in $\boldsymbol{v}$ and using the same logic,

$$\langle v_xv_y\delta r_y\rangle=0,\ \text{ but }\ \langle v_x^2\delta r_y\rangle=nTX_y. \tag{26}$$

The next rule may seem arbitrary,

$$\langle v_x^2\delta r_x\rangle=nTX_x, \tag{27}$$

because we could have written $\langle v_x^2 \delta r_x \rangle = \langle v_x \rangle \langle v_x \delta r_x \rangle$, and interpret the second factor as D. But this would mean assuming that v_x is independent of $v_x \delta r_x$. Equations (26) and (27) are usually obeyed within 5%.

It is straightforward to apply this closure hypothesis to the streaming fluxes. Putting the streaming fluxes into the hydrodynamic equations, we have

$$\frac{\partial \boldsymbol{X}}{\partial t} + \frac{1}{2}\boldsymbol{\nabla} D = \boldsymbol{U},$$

$$\frac{\partial \boldsymbol{U}}{\partial t} + \frac{1}{2}\boldsymbol{\nabla} E = 0,$$

$$\frac{\partial D}{\partial t} + T\boldsymbol{\nabla}\cdot\boldsymbol{X} = E,$$

$$\frac{\partial E}{\partial t} + T\boldsymbol{\nabla}\cdot\boldsymbol{U} = 0. \tag{28}$$

We can now explain the existence of two shear modes and four sound modes at each wavelength. If we assume that the hydrodynamic fields vary only in y, two equations decouple from the other four:

$$\frac{\partial X_x}{\partial t} = U_x,$$

$$\frac{\partial U_x}{\partial t} = 0. \tag{29}$$

These equations describe the shearing modes.

The other four equations are

$$\frac{\partial X_y}{\partial t} + \frac{1}{2}\frac{\partial D}{\partial y} = U_y,$$

$$\frac{\partial U_y}{\partial t} + \frac{1}{2}\frac{\partial E}{\partial y} = 0,$$

$$\frac{\partial D}{\partial t} + T\frac{\partial X_y}{\partial y} = E,$$

$$\frac{\partial E}{\partial t} + T\frac{\partial U_y}{\partial y} = 0. \tag{30}$$

These equations resemble two sets of compressible Euler equations, coupled by the terms on the right-hand side. They have oscillating solutions with a frequency of $\sqrt{T/2}$.

C. Instability of the shearing mode

The Eqs. (29) and (30) are an incomplete description of the hydrodynamic Lyapunov modes for their solutions grow only linearly in time. The Lyapunov modes grow exponentially with time, the growth rate being the Lyapunov exponent. In this section, we show that the growth rate of the shear modes can be explained by the hydrodynamic fluxes. These fluxes also govern the decay of the usual hydrodynamic modes. If a shear is imposed on a fluid, there is a flux of momentum along the velocity gradient that reduces the magnitude of the shear. In the Navier-Stokes equations, this flux is represented by the viscosity.

The hydrodynamic fluxes have two components: the ''streaming'' flux F_{stream}, and the ''collisional'' flux F_{coll}. The streaming flux gives the transport of the conserved quantity by the free movement of the particles. It has already been included in Eqs. (28), (29), and (30). The collisional flux gives the transport of the conserved quantities during collisions. It is not included in the above equations, because they were derived from a Boltzmann equation. In the Boltzmann equation, the collisional flux must vanish because the two colliding particles are assumed to be at the same position. [In Eq. (17), both particles A and B are at $\boldsymbol{r}$.]

We can measure the different parts of hydrodynamic fluxes in a simulation. Just before each collision, we perform an orthonormalization on all the vectors, and measure $\langle v_y \delta r_x \rangle$, which is the streaming flux of X_x. Just after the collision, we orthonormalize again, and measure the collisional flux of X_x. If this is carried out long enough, we can determine the spatial dependences of the fluxes, and the picture shown in Fig. 8 emerges. In Fig. 8(a), we see that both the streaming and collisional flux tend to reduce the amplitude of the mode. When $\partial X_x/\partial y > 0$, the fluxes are negative, indicating that negative X_x is being transported towards the high X_x regions, reducing the amplitude of the perturbation. Therefore, the cause of the exponential growth of the perturbation is not to be found there. On the other hand, Fig. 8(b) shows that the collisional flux of U_x is positive when the gradient is positive, indicating a ''negative viscosity'' that leads to the exponential growth.

But why should the viscosity be negative? For an explanation, see Fig. 9. Imagine there is a region with $X_x > 0$ lying just above a region where $X_x < 0$, as shown in the figure. The gradient of X_x is positive. A typical particle emerges from the $X_x > 0$ region, and encounters a typical particle from the $X_x < 0$ region in a head-on collision. Each particle's $\delta\boldsymbol{r}$ and $\delta\boldsymbol{v}$ is as shown in the figure. The collision rule is such that after the collision, each particle's $\delta\boldsymbol{v}$ is amplified. If the collision is head on, each particle returns to its region of origin—with its original perturbation amplified. In this way, the gradient in X_x increases.

Examining the conjugate partners of the shearing exponents confirms this explanation. In accordance with Eq. (7), X_x and U_x have opposite signs. Since the $F_{\text{coll}}(U_x)$ is generated by gradients in X_x, it changes sign with respect to U_x, and becomes a downgradient flux that reduces the amplitude of the perturbation. All the other fluxes remain downgradient.

D. Calculation of the collisional fluxes

Having demonstrated the existence of a negative viscosity, we would now like to calculate it. To do so, we will use the Enskog equation, which is an extension of the Boltzmann equation to high densities. The Enskog equation has the same form as the Boltzmann equation, except the collision operator is modified to

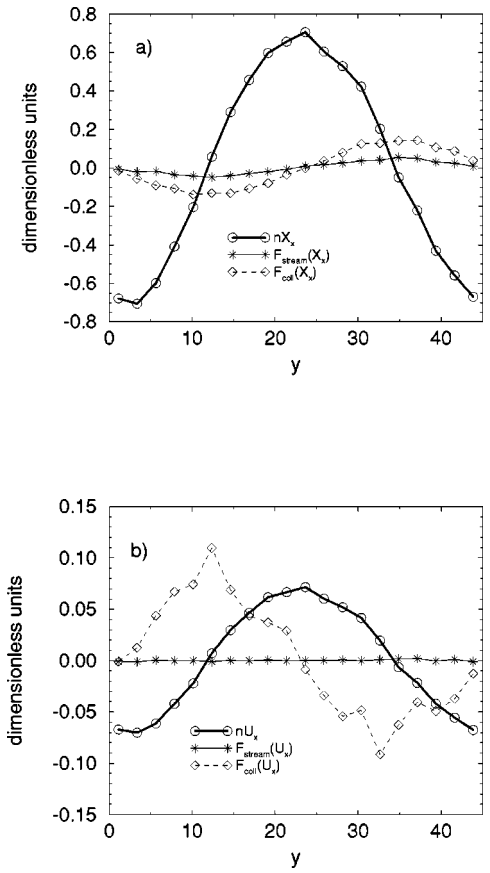

FIG. 8. X_x [panel (a)] and U_x [panel (b)] and their streaming fluxes, F_{stream}, and collisional fluxes, F_{coll}, for the Lyapunov mode $i=237$, shown in Fig. 5(d). The parameters are $N=120$, $L_x=15$, and $L_y=45$. The simulational domain was divided into 20 bins, each bin being L_x wide and $L_y/20$ high. Before each collision, we measured nU_x, nX_x, and the streaming fluxes. After the collision, the collisional fluxes were measured. This figure represents an average over 6000 collisions. All data are given in the dimensionless units discussed in Sec. I C.

$$\mathcal{C}_E=\chi\sigma\int \phi_A(\boldsymbol{r})\phi_B(\boldsymbol{r}_B)[\,\delta(\boldsymbol{q}_A'-\boldsymbol{q})-\delta(\boldsymbol{q}_A-\boldsymbol{q})]V \times\cos\theta d\boldsymbol{q}_A d\boldsymbol{q}_B d\theta. \tag{31}$$

Two changes have been made to the Boltzmann collision integral in Eq. (17) to yield this expression. First of all, a factor $\chi>1$ has been added to account for the increase in collision frequency due to excluded volume. We use [13]

$$\chi=\frac{1-(7\nu/16)}{(1-\nu)^2}, \tag{32}$$

where ν is the density expressed as the fraction of the area covered by the disks. The second change is to take into account the fact that when two particles collide, they are at different positions. Thus, $\phi_B(\boldsymbol{r})$ in Eq. (17) has been replaced by $\phi_B(\boldsymbol{r}_B)$. These subtle changes introduce the possibility of calculating the collisional fluxes.

Next, we can expand $\phi_B(\boldsymbol{r}_B)$ in a Taylor series:

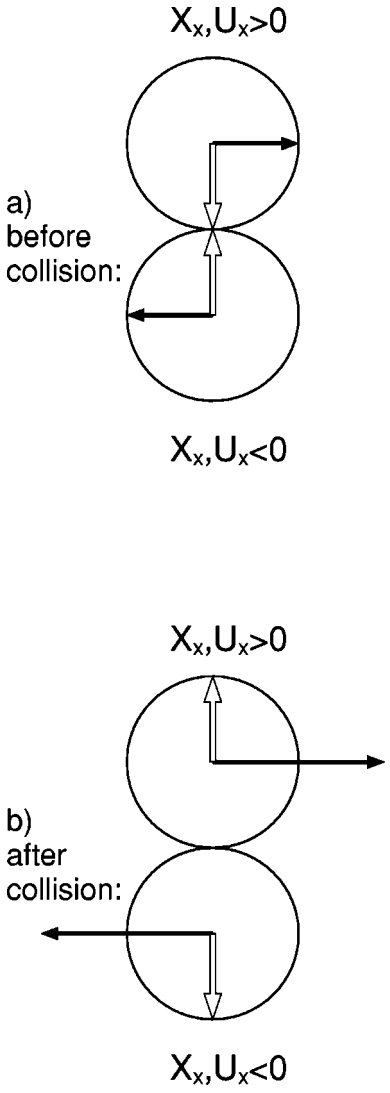

FIG. 9. The collisions that generate the anomalous viscosity. The solid arrows represent the Lyapunov coordinates $\delta\boldsymbol{r}$ and $\delta\boldsymbol{v}$, and the white arrow represents the velocities. The collision takes place in a region where the gradient of X_x is positive. The upper particle emerges from a region where $X_x>0$ and $U_x>0$; it has $\delta r_x>0$ and $\delta v_x>0$. It suffers a head-on collision with a particle emerging from the region with X_x, $U_x<0$. The collision is such that δv_x of each particle is augmented, and the particles return to their point of origin, thus amplifying the gradient.

$$\phi_B(\boldsymbol{r}_B)=\phi_B(\boldsymbol{r})+\sigma\hat{\boldsymbol{n}}\cdot\boldsymbol{\nabla}\phi_B(\boldsymbol{r})+\tfrac{1}{2}\sigma^2(\hat{\boldsymbol{n}}\cdot\boldsymbol{\nabla})^2\phi_B(\boldsymbol{r})+\cdots. \tag{33}$$

This enables us to split $\langle\psi\mathcal{C}\rangle$ into three parts,

$$\langle\psi\mathcal{C}_E\rangle=\langle\psi\mathcal{C}\rangle_0+\langle\psi\mathcal{C}\rangle_1+\langle\psi\mathcal{C}\rangle_2, \tag{34}$$

where

$$\langle\psi\mathcal{C}\rangle_0=\chi\sigma\int(\psi_A'-\psi_A)\phi_A\phi_B\omega_{AB}d\boldsymbol{q}_A d\boldsymbol{q}_B d\hat{\boldsymbol{n}},$$

$$\langle\psi\mathcal{C}\rangle_1=\chi\sigma\int(\psi_A'-\psi_A)\phi_A[\sigma\hat{\boldsymbol{n}}\cdot\boldsymbol{\nabla}\phi_B]\omega_{AB}d\boldsymbol{q}_A d\boldsymbol{q}_B d\hat{\boldsymbol{n}},$$

$$\langle \psi \mathcal{C} \rangle_2 = \chi\sigma \int (\psi_A' - \psi_A)\phi_A[(\sigma^2/2) \times (\hat{\boldsymbol{n}}\cdot\boldsymbol{\nabla})^2\phi_B]\omega_{AB} d\boldsymbol{q}_A d\boldsymbol{q}_B d\hat{\boldsymbol{n}}, \quad (35)$$

where all the distribution functions are evaluated at $\boldsymbol{r}$. Note that $\langle \psi \mathcal{C} \rangle_0$ is simply the Boltzmann collision operator, multiplied by ψ and integrated over $\boldsymbol{q}$. As above, it vanishes when ψ is one of the conserved quantities in Eq. (11). Furthermore, for these ψ, the remaining two expressions can be written as a divergence of a flux:

$$\langle \psi \mathcal{C} \rangle_1 = \chi(\sigma^2/2)\boldsymbol{\nabla}\cdot \int \hat{\boldsymbol{n}}(\psi_A' - \psi_A)\phi_A\phi_B\omega_{AB} d\boldsymbol{q}_A d\boldsymbol{q}_B d\hat{\boldsymbol{n}},$$

$$\langle \psi \mathcal{C} \rangle_2 = \chi(\sigma^3/4)\boldsymbol{\nabla}\cdot \int \hat{\boldsymbol{n}}(\psi_A' - \psi_A)\hat{\boldsymbol{n}}\cdot[\phi_A\boldsymbol{\nabla}\phi_B - \phi_B\boldsymbol{\nabla}\phi_A] \times \omega_{AB} d\boldsymbol{q}_A d\boldsymbol{q}_B d\hat{\boldsymbol{n}}. \quad (36)$$

Thus we can write

$$\langle \psi \mathcal{C} \rangle = -\boldsymbol{\nabla}\cdot \boldsymbol{F}_{\rm coll}(\psi). \quad (37)$$

$\boldsymbol{F}_{\rm coll}$ is the collisional flux of the quantity ψ, and can be extracted from Eq. (36).

The collisional fluxes, Eq. (36), are linear in the Lyapunov coordinates, and thus can be calculated using the closure hypothesis. The calculations are very long, so we will show only one calculation in detail.

As noted above, the collision rule for $\delta\boldsymbol{r}$ has the same form as the collision rule for velocities. Therefore, one obtains fluxes with a familiar form

$$\boldsymbol{\nabla}\cdot\boldsymbol{F}_{\rm coll}(\boldsymbol{X}) = \frac{n\zeta}{2}\boldsymbol{\nabla}D - n\mu[\nabla^2\boldsymbol{X} + \boldsymbol{\nabla}(\boldsymbol{\nabla}\cdot\boldsymbol{X})], \quad (38)$$

where ζ and the ''viscosity'' μ are

$$\zeta = \frac{\pi}{2} n\chi\sigma^2, \quad \mu = \frac{\sqrt{\pi}}{60} n\chi\sigma^3 T^{1/2}. \quad (39)$$

For $\boldsymbol{F}_{\rm coll}(D)$, we have

$$\boldsymbol{\nabla}\cdot\boldsymbol{F}_{\rm coll}(D) = n\zeta\boldsymbol{\nabla}\cdot\boldsymbol{X} - n\kappa\nabla^2 D, \quad (40)$$

where the ''thermal conductivity'' κ is

$$\kappa = \frac{17\sqrt{\pi}}{48}\chi n\sigma^2 T^{1/2}. \quad (41)$$

As stated above, the collision rule for $\delta\boldsymbol{v}$ has two parts. One part has the same form as the collision rule for $\delta\boldsymbol{r}$. These pieces will give fluxes with the same form as in Eq. (38) and Eq. (40), except that $\boldsymbol{X}$ is replaced by $\boldsymbol{U}$ and D is replaced by E. The second part of f_v, however, gives new results. Denote the fluxes due to this part by $\boldsymbol{F}^*_{\rm coll}$. Evaluation of these integrals gives

$$\boldsymbol{F}^*_{\rm coll}(E) = 0, \quad (42)$$

but $\boldsymbol{F}_{\rm coll}(\boldsymbol{U}) \neq 0$. We will now evaluate this flux.

Considering only the change in $\delta\boldsymbol{v}$ provoked by the second term of $\boldsymbol{f}_v$ in Eq. (10), we have

$$\psi_A' - \psi_A = \sec\theta|\boldsymbol{v}_B - \boldsymbol{v}_A|\sigma^{-1}(\delta\boldsymbol{r}_B - \delta\boldsymbol{r}_A)\cdot\hat{\boldsymbol{u}}\hat{\boldsymbol{u}}'. \quad (43)$$

Inserting Eq. (43) into Eq. (36) gives

$$\boldsymbol{F}^*_{\rm coll}(\boldsymbol{U}) = -\chi(\sigma/2)\boldsymbol{\nabla}\cdot\int \hat{\boldsymbol{n}}(\delta\boldsymbol{r}_B - \delta\boldsymbol{r}_A)\cdot\hat{\boldsymbol{u}}\hat{\boldsymbol{u}}' \times \phi_A\phi_B V^2 d\boldsymbol{q}_A d\boldsymbol{q}_B d\hat{\boldsymbol{n}} - \chi(\sigma^2/4)\boldsymbol{\nabla}\cdot\int \hat{\boldsymbol{n}}(\delta\boldsymbol{r}_B - \delta\boldsymbol{r}_A)\cdot\hat{\boldsymbol{u}}\hat{\boldsymbol{u}}' \times[\phi_A\boldsymbol{\nabla}\phi_B - \phi_B\boldsymbol{\nabla}\phi_A]\cdot\hat{\boldsymbol{n}} V^2 d\boldsymbol{q}_A d\boldsymbol{q}_B d\hat{\boldsymbol{n}}, \quad (44)$$

Following Ref. [9], the first step is to take the integral over $\hat{\boldsymbol{n}}$, considering the velocities as fixed. In two dimensions, this amounts to integrating over θ. Taking the limits of integration as $-\pi/2 \leqslant \theta \leqslant \pi/2$ ensures that we consider only velocities such that $(\boldsymbol{v}_A - \boldsymbol{v}_B)\cdot\hat{\boldsymbol{n}} \geqslant 0$. We must express $\hat{\boldsymbol{n}}$ in terms of $\hat{\boldsymbol{u}}$ and $\hat{\boldsymbol{v}}$, where $\hat{\boldsymbol{v}}$ is a unit vector pointing in the direction of $\boldsymbol{v}_A - \boldsymbol{v}_B$. From Fig. 7, we see $\hat{\boldsymbol{n}} = \hat{\boldsymbol{v}}\cos\theta - \hat{\boldsymbol{u}}\sin\theta$ and $\hat{\boldsymbol{u}}' = -\hat{\boldsymbol{v}}\cos 2\theta - \hat{\boldsymbol{u}}\sin 2\theta$. We carry out this substitution, and get a series of terms proportional to $\cos^n\theta\sin^m\theta$. Only terms containing an even power of $\sin\theta$ survive the integration over θ. This is sufficient to show that the first term vanishes. Equation (44) becomes

$$\boldsymbol{F}^*_{\rm coll}(\boldsymbol{U}) = \frac{\chi\sigma^2\pi}{16}\int \{(\hat{\boldsymbol{v}}\hat{\boldsymbol{v}} + \hat{\boldsymbol{u}}\hat{\boldsymbol{u}})(\boldsymbol{S}\cdot\hat{\boldsymbol{u}}) + (\hat{\boldsymbol{u}}\hat{\boldsymbol{v}} - \hat{\boldsymbol{v}}\hat{\boldsymbol{u}})(\boldsymbol{S}\cdot\hat{\boldsymbol{v}})\} \times(\delta\boldsymbol{r}_B - \delta\boldsymbol{r}_A)\cdot\hat{\boldsymbol{u}} V^2 d\boldsymbol{q}_A d\boldsymbol{q}_B. \quad (45)$$

We have written $\boldsymbol{S} = \phi_A\boldsymbol{\nabla}\phi_B - \phi_B\boldsymbol{\nabla}\phi_A$ to lighten the notation. Now, we do the integration over the Lyapunov coordinates, using the closure hypothesis given in Sec. III B. Since the Lyapunov coordinates appear with an even function of the velocities, we average the $\delta\boldsymbol{r}$'s to $\boldsymbol{X}$. (Recall that $\hat{\boldsymbol{u}}$ and $\hat{\boldsymbol{v}}$ are determined by the velocities.) The result is

$$\boldsymbol{F}_{\rm coll}(\boldsymbol{U}) = \frac{\chi\sigma^2\pi}{8}\int\int \{\mathbf{1}(\hat{\boldsymbol{v}}\cdot\boldsymbol{\nabla}) + \boldsymbol{J}(\hat{\boldsymbol{u}}\cdot\boldsymbol{\nabla})\} \times(\hat{\boldsymbol{u}}\cdot\boldsymbol{X}) f_A f_B V^2 d\boldsymbol{v}_A d\boldsymbol{v}_B. \quad (46)$$

Note that $\hat{\boldsymbol{v}}\hat{\boldsymbol{v}} + \hat{\boldsymbol{u}}\hat{\boldsymbol{u}} = \mathbf{1}$ and $\hat{\boldsymbol{u}}\hat{\boldsymbol{v}} - \hat{\boldsymbol{v}}\hat{\boldsymbol{u}} = \boldsymbol{J}$, where

$$\boldsymbol{J} = \begin{pmatrix} 0 & -1 \\ 1 & 0 \end{pmatrix}$$

is a matrix that rotates a vector by 90°. Now, we change variables to $\boldsymbol{v}_+ = (\boldsymbol{v}_A + \boldsymbol{v}_B)/\sqrt{2}$ and $\boldsymbol{v}_- = (\boldsymbol{v}_A - \boldsymbol{v}_B)/\sqrt{2}$, and do the integral over the velocities. The unit vectors are just functions of the angle of $\boldsymbol{v}_-$. The result is

$$\boldsymbol{F}_{\rm coll}(\boldsymbol{U}) = -n\xi\left[\mathbf{1}\boldsymbol{\nabla}\cdot\boldsymbol{X} + \boldsymbol{J}\left(\frac{\partial X_y}{\partial x} - \frac{\partial X_x}{\partial y}\right)\right], \tag{47}$$

where ξ is a new tranport coefficient

$$\xi = \frac{\pi}{4}\chi\sigma^2 nT. \tag{48}$$

As we show below, Eq. (47) gives a term that accounts for the growth of the shear modes.

E. A quantitative estimate of the shearing exponents

Putting the computed collisional fluxes into Eq. (29), the governing equations of the shear mode become

$$\frac{\partial X_x}{\partial t} = U_x + \mu\frac{\partial^2 X_x}{\partial y^2},$$

$$\frac{\partial U_x}{\partial t} = \mu\frac{\partial^2 U_x}{\partial y^2} - \xi\frac{\partial^2 X_x}{\partial y^2}. \tag{49}$$

Since Eq. (49) is linear, we can get a dispersion relation by inserting

$$X_x = \hat{X}e^{\lambda t + iky}, \quad U_x = \hat{U}e^{\lambda t + iky}. \tag{50}$$

Putting this solution into Eq. (49) and eliminating $\hat{X}$ and $\hat{U}$ gives

$$\lambda = \pm\sqrt{\xi}k - \mu k^2. \tag{51}$$

The first term above corresponds exactly to what is observed. Taking the positive sign, we have the growing mode, and taking the negative sign, we have its conjugate partner. Furthermore, the growth rate is linear in k. The second term, however, is not what is observed. In the Lyapunov spectra, the sum of each exponent and its conjugate partner is exactly 0. But according to Eq. (51), this is not so. The sum of each mode and its conjugate partner is $-2\mu k^2 < 0$. Therefore, it is tempting to dismiss the second term, because it is not time reversible. But if we set $\mu = 0$ in Eq. (49), it seems we should also set $\xi = 0$. We do not currently have any satisfactory reason for keeping ξ but eliminating μ.

Another objection to Eq. (51) is that it predicts that short wavelength instabilities grow most rapidly, and therefore the long wavelength patterns observed in Fig. 5 are unstable, and would not be observed. This is partly correct—the patterns in Fig. 5 are unstable, but they are observed because the periodic orthonormalization removes the components at higher wave numbers. It is an implicit assumption of the theory that this is the only effect of the orthonormalization.

We now make a quantitative comparison between the theory and the simulation. Comparing Eq. (51) with Eq. (8), we see

$$c_\lambda = 2\pi\sqrt{\xi}. \tag{52}$$

In Fig. 10, we present a comparison of the theory with the observed values. Close agreement between the theory and the simulation is not expected because the theory neglects the streaming fluxes. In particular, the collisional flux must vanish at $\nu = 0$, so theoretical curve in Fig. 10 must pass through the origin. The smallness of the streaming flux in Fig. 8 ($\nu = 0.56$) suggests that a calculation of the streaming fluxes is not enough to account for the difference between theory and simulation. Nevertheless, Fig. 10 shows that the kinetic theory is a good first step in the quantatative explanation of the shear modes.

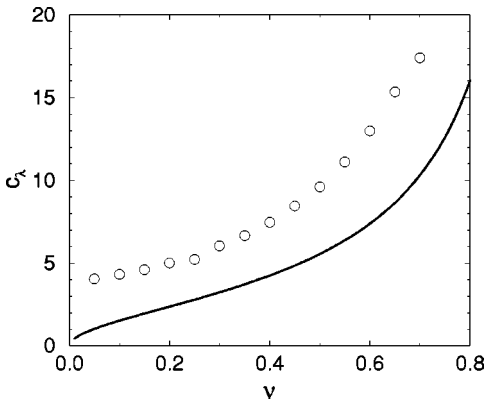

FIG. 10. A comparison of computed and observed c_λ. The circles are the observed values of c_λ from Fig. 6 for the shearing mode, and the solid line is Eq. (52).

F. The sound modes

Adding the collisional fluxes, the sound mode equations become

$$\frac{\partial X_y}{\partial t} + \frac{1}{2}(1+\zeta)\frac{\partial D}{\partial y} = U_y + \mu\frac{\partial^2 X_y}{\partial y^2},$$

$$\frac{\partial U_y}{\partial t} + \frac{1}{2}(1+\zeta)\frac{\partial E}{\partial y} = \mu\frac{\partial^2 U_y}{\partial y^2} + \xi\frac{\partial^2 X_y}{\partial y^2},$$

$$\frac{\partial D}{\partial t} + T(1+\zeta)\frac{\partial X_y}{\partial y} = E + \kappa\frac{\partial^2 D}{\partial y^2},$$

$$\frac{\partial E}{\partial t} + T(1+\zeta)\frac{\partial U_y}{\partial y} = \kappa\frac{\partial^2 E}{\partial y^2}. \tag{53}$$

Unfortunately, these equations do not produce unstable modes, so the growth of the sound waves is not explained by the kinetic theory. This can also be verified in simulations, but it is more difficult to do, because the sound modes are continually moving, so one cannot take a long time average of the fluxes to see their relation to the fields. This difficulty can be overcome by calculating the correlation function between each field and its fluxes. However, there is another problem, because the fluxes are dominated by the movement of the sound wave, and not by its growth or decay. But if we add the correlation functions of all four sound modes together, the fluxes responsible for this translation will then

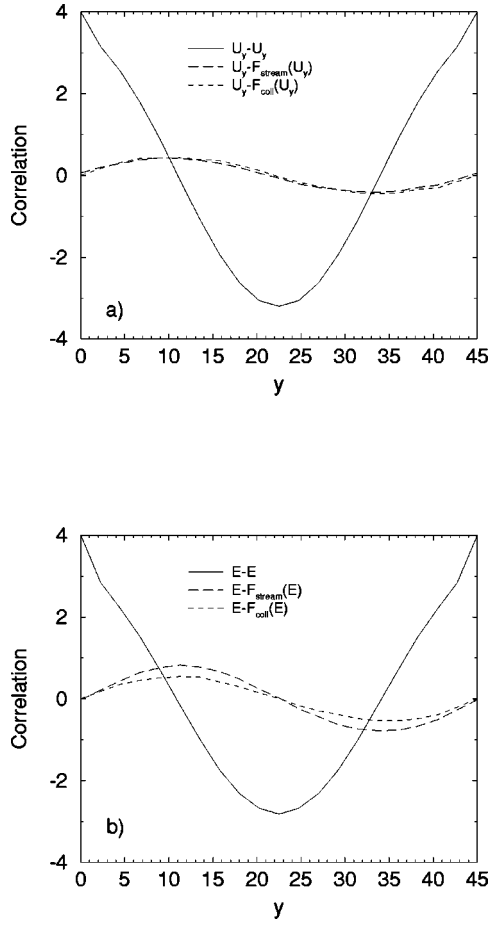

FIG. 11. The spatial correlations between U_y [panel (a)] and E [panel (b)] and their fluxes. The solid lines are the U_y or E space autocorrelation functions. The dotted lines are the spatial correlation functions of the fields with their fluxes. To obtain this figure, 200 different profiles of U_y, E, and their fluxes were constructed for each of the four sound modes. The spatial correlation function was calculated for each profile, and all the profiles for a single mode were averaged together to give that mode's correlation functions. Then the corresponding functions of the four modes were added together to give these curves. The system used to construct this figure is the one shown in Figs. 3 and 5.

cancel out, because two sound modes propagate in the positive y direction and the other two in the negative direction.

The results for U_y and E are shown in Fig. 11. We see that in both cases, the flux has the opposite sign of the gradient. Therefore all fluxes are dissipative, tending to reduce the amplitude of the perturbation. The kinetic theory approach does not explain the growth of the sound modes.

Equation (53) predicts soundlike waves at two different frequencies,

$$\omega = i\left[c_*^2 - \frac{\xi}{2} \pm \sqrt{2c_*^2\xi + \xi^2/4}\right]^{1/2} k + O(k^2), \qquad (54)$$

where $c_* = \sqrt{T/2}(1+\zeta)$, which would be the sound speed if we set the right-hand sides of Eq. (53) to 0. In Fig. 12, we compare the observed values of ω/k (the phase velocity of the waves) to Eq. (54). The observed sound speed is not

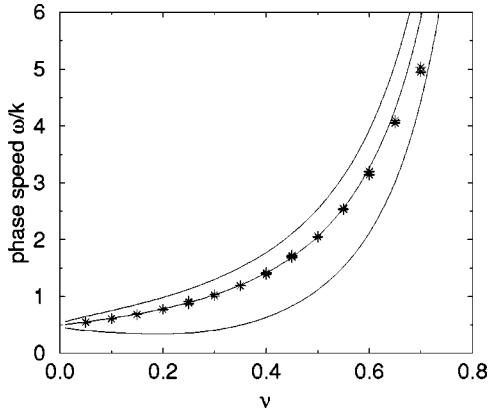

FIG. 12. A comparison of the theoretical and observed sound speeds. The upper and lower theoretical curves are the predicted sound speeds. The middle curve is c_*, the predicted sound speed with $\xi = 0$.

equal to either of the two values predicted by Eq. (54), but it is very close to c_*. (Note that c_* contains both the streaming and the collisional fluxes, unlike our estimate for the growth rate of the shear mode in Fig. 10.) The agreement between c_* and the observed values is too good to simply be a coincidence. Therefore, we believe that the left-hand sides of Eq. (53) correctly describes the sound modes, but the diffusive terms on the right-hand sides do not seem to be correct. This is especially true for the term proportional to ξ, which modifies the predicted sound speed in a way that is not observed. But there seems to be no reason why we should set $\xi = 0$ here, and not in Eq. (51). Note that the periodic orthogonalization constrains the sound waves to have the same frequency, because they must always remain orthogonal to one another. This fact has not been taken into account in Eq. (54). Finally, we note that the most doubtful closure assumption, Eq. (24), concerns only the sound modes.

The observed sound speed c_* is very close to half of the observed sound speed [2]. This is because the pressure of the the hard disk fluid can be written

$$p = (1+\zeta)nT. \qquad (55)$$

Therefore, the left-hand sides of Eq. (53) are closely related to the compressible Euler equations, with X_y and U_y in the role of the velocity, and with D and E as the temperature. Certain numerical factors, such as the 1/2 in the equations for X_y and U_y, reduce the frequency by a factor of 2.

This observation raises the question of the relation between the transport coefficients and the Lyapunov exponents. Is it possible to extract the transport coefficients from certain hydrodynamic Lyapunov exponents? This paper suggests that it is not possible. We were able to estimate the exponent associated with the shearing mode [Eq. (51) and Fig. 10]. The origin of this exponent's growth is the upgradient transfer of $\delta\boldsymbol{v}$ due to the second term of Eq. (10), the $\delta\boldsymbol{v}$ collision rule. This term has no analog in velocity collision rule, Eq. (1). The viscosity of the hard disk fluid has entirely different origin. It is due to the downgradient transfer of momentum during collisions, and the correlations between v_x and v_y.

IV. CONCLUSION

We have presented an explanation for the ''hydrodynamic'' Lyapunov modes first observed by Posch and Hirschl [2]. We consider the components of the Lyapunov vector associated with each particle to be quantities carried by that particle. We then look at how these quantities change during a collision, and we find that certain combinations of these quantities are conserved. The hydrodynamic Lyapunov modes arise from these new conservation laws in the same way the hydrodynamic modes arise from the conservation of mass, momentum, and energy. This is the central idea of this paper. We attempted to apply this idea in more detail by defining a generalized Boltzmann equation. We are able to explain a number of properties of the exponents: the existence of two ''shear'' modes and four ''sound'' modes for each wave number, and an estimate of the Lyapunov exponent associated with the shearing mode. On the other hand, the statistical approach of the Boltzmann equation introduces certain terms that are not observed. Neither is our theory able to explain the growth of the sound modes (although the phase speed of the waves is correctly predicted). This combination of success and failure leads us to the conclusion that the link between the conserved quantities and the hydrodynamic Lyapunov modes is correct, but it must be elaborated in a way different than the kinetic theory approach presented here. An improved theory may have to explicitly treat the orthonormalization of the displacement vectors $\delta\mathbf{\Gamma}_i$. In our theory, we do not consider the orthonormalization, assuming that its only effect is to suppress short wavelength perturbations. Another possible improvement would be to relax the isotropy assumption of Eq. (24).

This work also suggests that a simple relation between the hydrodynamic Lyapunov exponents and the transport coefficients does not exist. The hydrodynamic exponents arise from a term in the velocity space displacement collision rule, Eq. (10), which has no analog in the velocity collision rule, Eq. (1).

ACKNOWLEDGMENTS

We thank Christoph Dellago, Rodrigo Soto, Pierre Gaspard, Stefano Ruffo, and Bill Hoover for several helpful discussions. We also thank Harald Posch for providing us with Ref. [2] before its publication. We thank the Center National de la Recherche Scientifique for funding a part of this work.

[1] Ch. Dellago, H.A. Posch, and W.G. Hoover, Phys. Rev. E **53**, 1485 (1996); Ch. Dellago and H.A. Posch, Physica A **240**, 68 (1997).
[2] H.A. Posch and R. Hirschl, in *Hard-Ball Systems*, edited by D. Szasz (Springer Verlag, Berlin, 2000).
[3] Lj. Milanović and H.A. Posch, Chaos **8**, 455 (1998).
[4] S.D. Stoddard and J. Ford, Phys. Rev. A **8**, 1504 (1973).
[5] W.G. Hoover, *Time Reversibility, Computer Simulation and Chaos* (World Scientific, Singapore, 1999).
[6] E.G.D. Cohen, Physica A **213**, 293 (1995); E.G.D. Cohen, in *Dynamics: Models and Kinetic Methods for Non-Equilibrium Many Body Systems*, Vol. 371 of *NATO Series E: Advanced Study Institute Applied Sciences*, edited by J. Karkheck (Kluwer, Amsterdam, 2000).
[7] J.R. Dorfman and P. Gaspard, Phys. Rev. E **51**, 28 (1995).
[8] J.R. Dorfman and H. van Beijeren, Physica A **240**, 12 (1997).
[9] S. Chapman and T.G. Cowling, *The Mathematical Theory of Non-Uniform Gases* (Cambridge University Press, Cambridge, England, 1939).
[10] G. Benettin, L. Galgani, A. Giorgilli, and J.M. Strelcyn, Meccanica **15**, 9 (1980).
[11] A. Wolf, J.B. Swift, H.L. Swinney, and J.A. Vastano, Physica D **16**, 285 (1985).
[12] J.P. Eckman and Omri Gat, J. Stat. Phys. **98**, 775 (2000).
[13] L. Verlet and D. Levesque, Mol. Phys. **44**, 969 (1982).